International Journal of Fatigue 100 (2017) 285–295

Contents lists available at ScienceDirect

International Journal of Fatigue

journal homepage: www.elsevier.com/locate/ijfatigue

Environmentally assisted fatigue behaviour of stress relieved metal inert gas (MIG) AA5083 welds in 3.5% NaCl solution

M.N. Ilman [a,*], N.A. Triwibowo [a], A. Wahyudianto [a], M.R. Muslih [b]

[a] Department of Mechanical and Industrial Engineering, Universitas Gadjah Mada (UGM), Yogyakarta, Indonesia
[b] National Nuclear Energy Agency of Indonesia (BATAN), Serpong, Banten, Indonesia

ARTICLE INFO

Article history:
Received 31 December 2016
Received in revised form 24 March 2017
Accepted 25 March 2017
Available online 30 March 2017

Keywords:
Aluminium weld
Stress relieving
Passivity
Environmentally assisted fatigue

ABSTRACT

Environmentally assisted fatigue crack propagation behaviour of metal inert gas (MIG) welded AA5083 joints under stress relieving treatment has been investigated. In this study, 'in-process' stress relieving treatment, namely static thermal tensioning was applied during MIG welding process. Subsequently, fatigue crack propagation tests were performed in 3.5% NaCl solutions with and without a chromate inhibitor. A sinusoidal loading wave form was used in these fatigue tests with stress ratio, R and frequency, f of 0.1 and 8 Hz respectively. For complementary tests, residual stress measurements were conducted using neutron diffraction method whereas effect of corrosive environments was assessed using potentiodynamic polarisation technique. Results showed that electrochemical corrosion characteristics of the weld metals under stress relieving treatment were improved marked by the presence of anodic passivation regions in potentiodynamic polarisation curves with reduced corrosion rates. Moreover, synergistic effect of compressive residual stress and repassivation of the weld joints seemed to inhibit environment fatigue crack propagation.

1. Introduction

Increasing interest in the use of AA5083 and the 5xxx series aluminium alloys for lightweight structures such as ship construction is driven by their excellent properties. The alloys provide many benefits such as relatively high strength to weight ratio which helps to produce light-weight structures for increased performance (e.g. speed and manoeuvrability), good weldability, good general corrosion resistance in marine environment and also nonmagnetic and nontoxic properties [1,2]. The AA5083 is an Al-4.5%Mg-1%Mn wrought alloy in which its strength is increased through two strengthening mechanisms, i.e. solid solution strengthening by a magnesium (Mg) addition and strain hardening [3].

In aluminium ship fabrication, welding is one of the most critical manufacturing processes since around 60–65% of the total production cost for an average ship consists of assembly of plates and welding. Up to now, metal inert gas (MIG) and tungsten inert gas (TIG) welding processes are still the most common joining techniques for aluminium alloys [4] despite more advanced joining processes are now being developed. Unfortunately, welding of aluminium alloys using such arc welding processes often produces problems such as distortion and residual stress. The presence of residual stresses in welds can cause fatigue failure, brittle fracture and stress corrosion cracking [5]. Numerous works have been carried out to minimise distortion and residual stress using mechanical [6–8] or thermal treatments [9,10] where these two techniques can be applied either prior to/during welding known as in-process welding [11,12] or after welding (post weld treatments) [13,14].

Considerable researches have been conducted with the aim of gaining better understanding of corrosion characteristics in welds under stress relieving treatments. Several reports show that either post weld heat treatment (PWHT) [15,16] or mechanical treatments such as peening techniques [17,18] can modify corrosion behaviour in welds due to changes in electrochemical properties, i.e. stable protective films and the formation of compressive residual stresses.

In construction applications, metallic welded structures such as ships are often subjected to dynamic loads and at the same time, they are exposed to corrosive environment. Under such a condition, corrosion fatigue often known as environmentally assisted fatigue may occur. In general, factors affecting environmentally assisted fatigue in metallic materials include load frequency [19–21], temperature [22–24], metallurgical factors [25–27] and environment conditions [28–32]. In recent years, a number of research works on corrosion fatigue of AA5083 and its welding condition

* Corresponding author.
E-mail address: ilman_noer@ugm.ac.id (M.N. Ilman).

http://dx.doi.org/10.1016/j.ijfatigue.2017.03.041
0142-1123/

has been conducted. It has been reported that fatigue of welded aluminium alloy AA5083 in a seawater environment often initiates at pores [33]. Another investigation [34] has shown that corrosion fatigue of heat treated 6061-T651 aluminium alloy welded using ER5183 filler alloy in 3.5% NaCl solution is initiated by corrosion pits which nucleate on precipitates. More recently, the work of Sharma et al. [35] on conventional AA5083-H111 and ultra-fine grained (UFG) Al-Mg alloys have shown that pitting corrosion (inclusions precipitates) acts as stress concentrator in both alloys. According to the authors, the corrosion fatigue in such alloys takes place via two mechanisms. First, at high stress ranges, slips promote dissolution and hydrogen embrittlement. Secondly, pitting becomes the prevailing mechanism as the applied stress value is low.

As stated previously, several works have been directed at the understanding the effect of stress relieving treatments on electrochemical corrosion characteristics in aluminium welded joints. However, further effect of these treatments on fatigue crack propagation behaviour of aluminium welds in aqueous environments, in particular 3.5% NaCl solution, is not well documented. In the present paper, modification of residual stress by stress relieving treatment and its effect on environmentally assisted fatigue crack propagation in 3.5% NaCl solution is studied for metal inert gas AA5083 welded joints.

2. Experimental procedure

2.1. Materials and welding procedure

In this study, 5083 aluminium alloy plates with the size of 3 mm × 100 mm × 400 mm were butt welded along 400 mm long using metal inert gas (MIG) welding process with a filler metal used was ER5356. The chemical compositions of the 5083 aluminium alloy plates and ER5356 filler metal are given in Table 1.

Welding parameters used in this study are shown in Table 2. In-process stress relieving treatment, namely static thermal tensioning (STT) was applied during welding as shown in Fig. 1. The electric heaters which acted as secondary heat sources were placed at both sides of the weld line and simultaneously, the bottom of the weld zone was quenched using water flow inside the copper backing bars to create thermal gradient. Such a condition was expected to provide stretching effect (thermal tensioning) to reduce distortion and residual stress. The centre to centre distance between the two heaters was 120 mm and the heating temperature was set at 250 °C. Details of this experiment are given elsewhere [10]. The mechanical properties of the weld metals after welding are listed in Table 3.

2.2. Microscopical examinations

Microstructural examinations were directed at the transverse sections of the weld joints which consisted of various zones, namely weld metal (WM), heat affected zone (HAZ) and base metal (BM) using optical microscopy. Each sample for metallographic studies was first cut perpendicular to the welding direction then mounted in epoxy resin, mechanically ground and polished, and finally etched using Keller reagent (2 ml HF, 3 ml HCl, 5 ml HNO_3 and 190 ml H_2O).

Table 2
Materials and welding parameters.

Parameter	Values
Filler Material	ER5356
Wire diameter	0.8 mm
Wire speed	9 m/min (150 mm/s)
Shielding gas	Argon (Ar)
Gas flow	14 L/min
Voltage	20 V
Current	100 A
Welding speed	10 mm/s
Water flow	1200 L/h

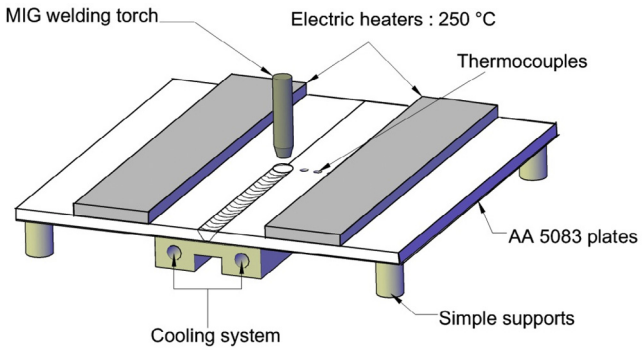

Fig. 1. A schematic drawing of static thermal tensioning (STT) treatment applied during welding.

Table 3
Mechanical properties of the weld metals.

Material	Tensile strength (MPa)	Yield stress (MPa)	Elongation (%)
As welded	216	152	10.4
Stress relieved	255	184	10.3
AA5083 base metal	298	230	20.1

2.3. Residual stress measurements

Residual stress measurements using neutron diffraction method were undertaken at the National Nuclear Energy Agency of Indonesia (BATAN). In this study, residual stress profiles of the welded AA5083 plates were measured along transverse distance from the weld centre line with the location of measurements was taken at the middle part of the welded plate length. The neutron wavelength used was 1.83375 Å and it was diffracted on (311) reflection at the detector angle (2θ) of approximately 96.5°. A gauge volume size, typically 8 mm^3 having dimension of 2 × 2 × 2 mm^3 was used in this investigation. Lattice measurements were made in the principal stress directions, namely x (longitudinal), y (transverse) and z (normal) directions. The residual strains (ε_{hkl}) were determined through the equation [36]:

$$\varepsilon_{hkl} = \frac{d_{hkl} - d_o}{d_o} \quad (1)$$

where d_{hkl} and d_o are stressed and stress-free lattice parameters respectively. By using tensors of 2nd rank, the strains (ε_{ii}) measured

Table 1
Chemical compositions (wt%) of AA 5083 plates and ER 5356 filler metal.

Material	Mg	Mn	Si	Fe	Cr	Cu	Zn	Ti	Al
AA 5083	4.5	0.65	0.26	0.22	0.09	0.09	0.06	0.03	Bal.
ER 5356	4.5–5.5	0.05–0.20	0.25	0.40	0.05–0.20	0.10	0.10	0.06–0.20	Bal.

in the principal directions were converted to residual stresses (σ_{ii}) using Hooke's law as given in Eq. (2).

$$\sigma_{ii} = \frac{E}{1+v}\varepsilon_{ii} + \frac{vE}{(1+v)(1-2v)}\Sigma\varepsilon_{jj} \quad (2)$$

where subscript i represents triaxial principal directions with $i = x, y, z$. In the present investigation, Young's modulus (E) for 5083 aluminium alloy was taken as 70 GPa whereas Poisson's ratio (v) used was 0.3. Of note is that errors of these residual measurements were estimated to be ±20 MPa.

2.4. Corrosion tests

Corrosion characteristics of the welds under study were assessed using potentiodynamic polarisation method. Circular-shaped specimens with the dimension of 15 mm in diameter and 2 mm in thickness were taken from the weld metal regions. After grinding and polishing, each specimen which acted as working electrode was immersed in 3.5% NaCl solutions with and without sodium chromate (Na_2CrO_4) inhibitor whereas reference and counter electrodes used were saturated calomel electrode (SCE) and platinum (Pt) respectively. The use of chromate inhibitor was intended to study corrosion characteristics in particular passive film stability in the AA5083 welded joints. For this reason, the percentages of Na_2CrO_4 in 3.5% NaCl solutions were varied, typically of 0.1, 0.3 and 0.5%. Each specimen was polarised either anodically or cathodically in the range of −1.10 to +0.1 V at a scan rate of 0.1 mV/s using a pontentiostat/galvanostat (Model EG&G 273). Based on the results obtained from potentiodynamic polarisation tests, the inhibition efficiency (η) can be calculated using the following equation [37,38]:

$$\eta(\%) = \frac{i_o - i}{i_o} \times 100 \quad (3)$$

where i and i_o are corrosion rates with and without inhibitor respectively.

2.5. Corrosion fatigue tests

Environmentally assisted fatigue crack propagation (EAFCP) studies were conducted by immersing each fatigue specimen in a transparent acrylic resin chamber containing corrosive media as shown in Fig. 2. The corrosive media used were varied, i.e. 3.5% NaCl solutions with and without 0.3% Na_2CrO_4 addition. Of note is that the interactions between residual stress and Na_2CrO_4 inhibitor are better studied as the amount of Na_2CrO_4 is around 0.3%. If the inhibitor addition is too low, it cannot produce protective films sufficiently and therefore, the inhibitor does not have a significant influence on EAFCP. In contrast, excessive inhibitor makes the cracked surface to become isolated from the corrosive media and again, the effect of environment is significantly reduced. In this investigation, fatigue tests in dry air were also performed as the reference. Each fatigue specimen was machined in the form of centre crack tension (CCT) specimen according to ASTM E-647 with an initial crack was made at the weld region and oriented parallel to the weldline.

In order to meet the low frequency regime for EAFCP to operate, the loading frequency should be below 10 Hz [3,39]. The loading frequency used in this study was 8 Hz with a stress ratio (R) of 0.1. This low R was expected to allow compressive residual stress to have most influence on fatigue crack growth, especially at low ΔK. After fatigue tests, fractographic studies were also conducted using scanning electron microscopy (SEM) equipped with energy dispersive X-ray (EDX) analysis. Fractographic studies were focused on the stable crack growth region, i.e. region II near threshold region.

3. Results and discussion

3.1. Weld microstructure

To gain comprehensive understanding of environmentally assisted fatigue crack propagation behaviour of MIG 5083 aluminium alloy weld joints, it is necessary to study the weld microstructures. Fig. 3 shows typical microstructures of the MIG AA5083 welded joint in as welded (untreated) condition. It can be seen that the weld metal (WM) region as shown in Fig. 3b is composed of equiaxed dendritic networks of α-phase (light-etched) which is the solid solution of Mg in Al whereas β-phase constituents (dark-etched) were precipitated within interdendritic arm spacings. The formation of β-phase is resulted from localised solute enrichment within interdendritic arm spacings due to solute redistribution during solidification. In an aluminium alloy such as AA 5083, partially melted zone (PMZ) exists along fusion line as shown in Fig. 3c. This region is located between weld metal (WM) which is fully melted fusion zone and unmelted heat

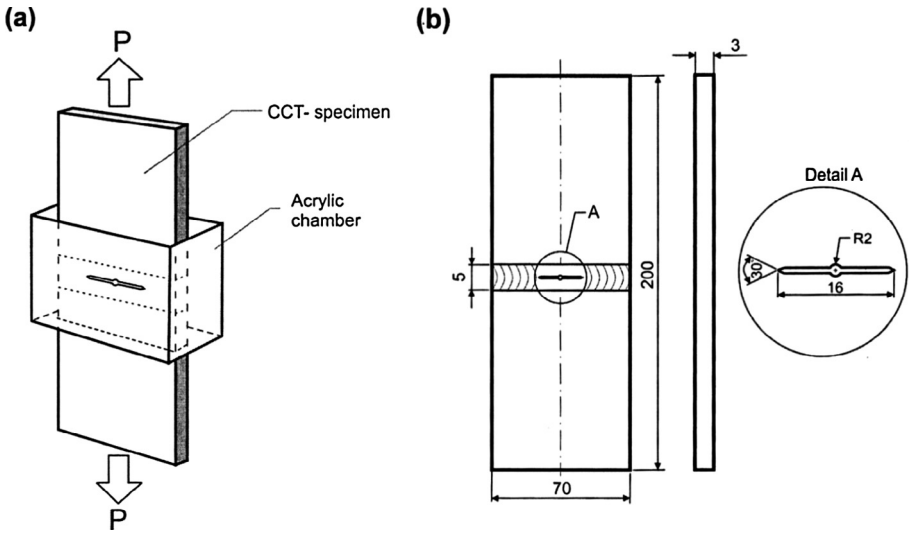

Fig. 2. An experimental set-up for corrosion fatigue test with a CCT-specimen.

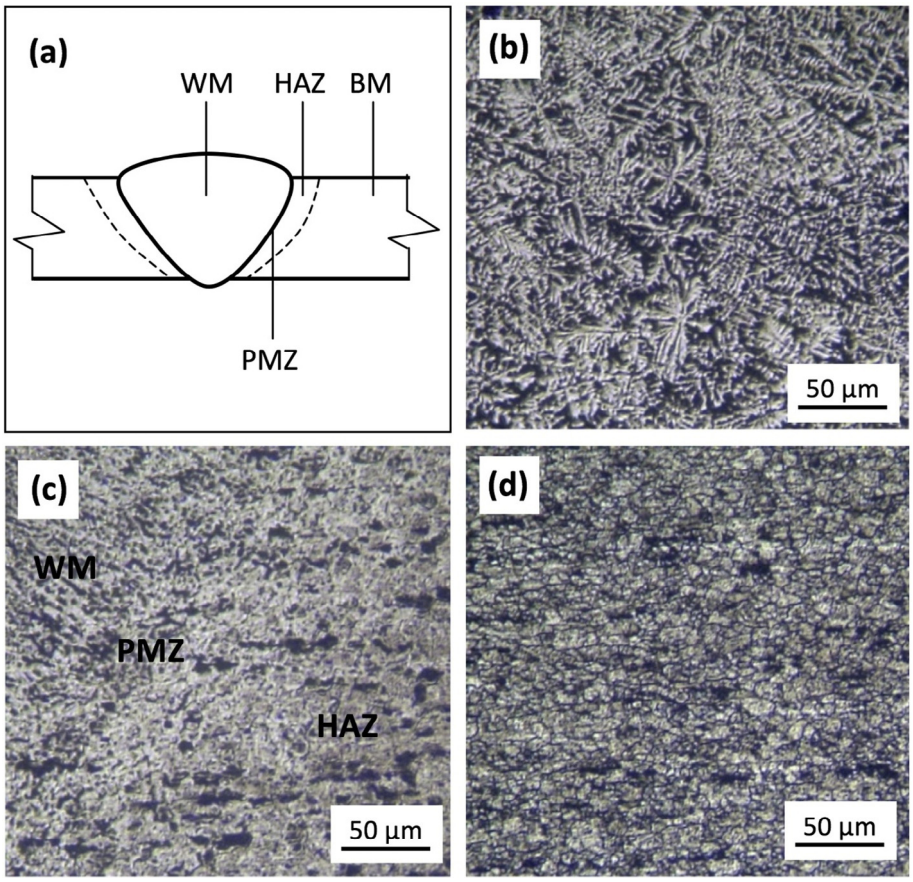

Fig. 3. (a) A weld profile with the corresponding microstructures: (b) weld metal (WM), (c) partially melted zone (PMZ)-heat affected zone (HAZ), and (d) base metal (BM) in as welded MIG 5083 aluminium alloy weld joint.

affected zone (HAZ). Subsequently, the region close to PMZ region is HAZ. The HAZ region is marked by the presence of coarse grained microstructure resulted from grain growth during welding. Another feature observed in the HAZ region is the presence of coarse precipitates (dark-etched), probably in the form of Al_3Mg_2 which formed during welding process. Furthermore, at the region far from the weld metal as shown in Fig. 3d, the effect of heat is diminished and the microstructure reveals fine grained structure with the grains are oriented parallel to rolling direction typical of wrought aluminium alloys. This region is known as unaffected base metal (BM).

It seems that there is close relationship between weld microstructure and mechanical properties. Referring to Table 3, it can be seen that the strengths of as welded and stress relieved weld metals are lower than their base metal. This is because the weld metals are cast products which usually have lower strength compared to wrought product such as base metal.

Of note is that the present investigation is focused on the weld metal region where a maximum tensile residual stress commonly forms at the weld metal region and this stress should be balanced by compressive residual stresses which form at areas away from the weld. Previous investigation [10] has shown that static thermal tensioning treatment strongly affects weld residual stress and distortion without producing significant changes in weld microstructure at the optical microscope scale.

3.2. Weld residual stresses

Results of longitudinal (parallel to the weld) and transverse (perpendicular to weld) residual stresses of MIG 5083 aluminium alloy welded plates are shown in Fig. 4. It can be seen that the longitudinal residual stress profile of as welded weld metal (Fig. 4a) is marked by the presence of relatively high tensile residual stress at weld centreline, typically of 85 MPa whereas the maximum residual stress is around 150 MPa formed at the region near the weld. The stress relieving treatment changes the tensile residual stress at the weld centre line to become compressive with the lowest value of −133 MPa at the weld centreline. Similar trends are observed in the transverse residual stresses (Fig. 4b) in which the transverse residual stresses in as welded condition are shifted towards more negative (compressive) stresses due to stress relieving treatment. It is interesting to note that in as welded condition (Fig. 4), the magnitude of tensile residual stress at the weld region and its adjacent area along longitudinal direction is higher compared to the residual stress along transverse direction. This may be attributed to the presence of restraint of dimensional changes, i.e. expansion and contraction/shrinkage during welding by unheated base metal where the degree of restraint in the longitudinal direction is higher than that in the transverse direction. Of note is that the maximum weld residual stress in the present study is lower than the yield stress of the weld metals as shown Table 3.

As reported previously [40,41], thermal gradient resulted from thermal tensioning treatment produces stretching effect (or thermal tensioning) which opposes the tensile residual stress developed during welding. As a result, the tensile residual stress is reduced and at a certain extent, the residual stress becomes compressive.

Considering the results of residual stress measurements, the distributions of longitudinal and transverse residual stresses in both as welded and stress relieving conditions are suggested as

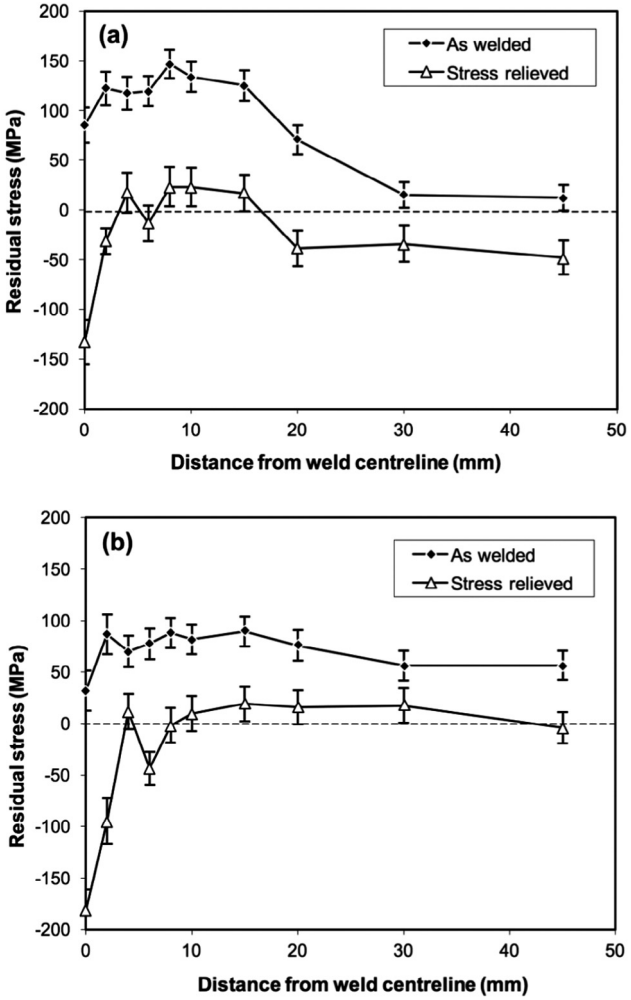

Fig. 4. Distribution of: (a) longitudinal residual stress and (b) transverse residual stress.

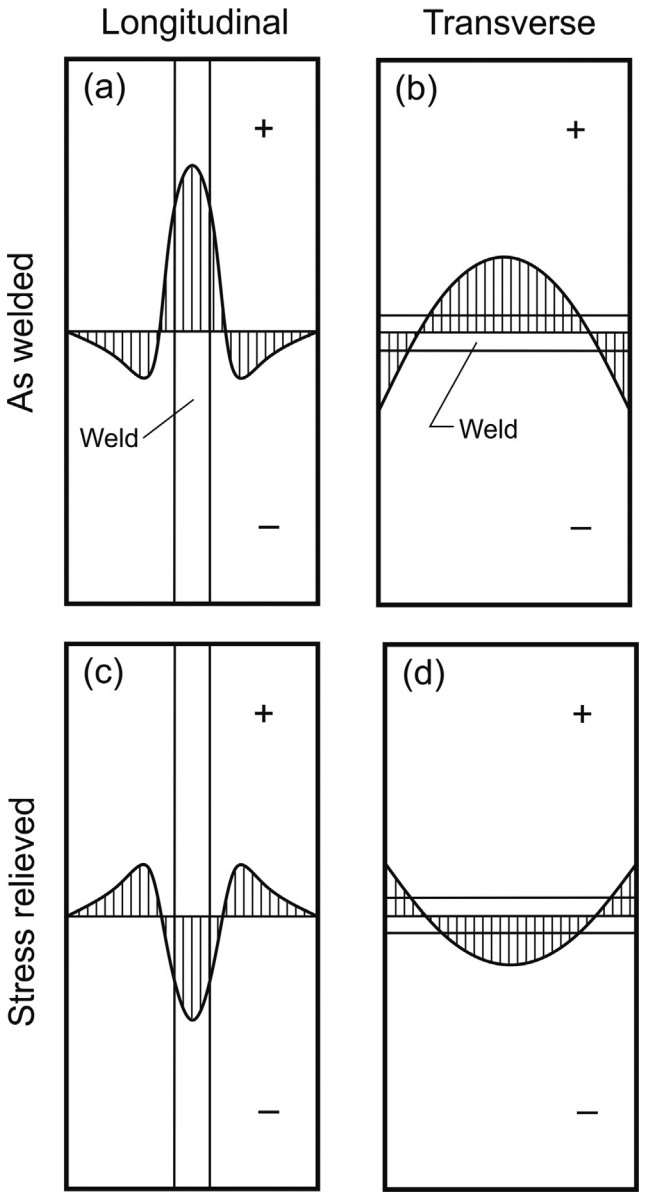

Fig. 5. Schematic representation of longitudinal and transverse residual stress profiles with and without stress relieving treatment.

shown in Fig. 5. In as welded condition as shown in Fig. 5a, the longitudinal residual stress profile is marked by the maximum tensile stress at the weld region which is balanced by compressive residual stresses at both sides of the weld region.

The distribution of transverse residual stress along the weld length is shown in Fig. 5b. It can be seen that the tensile transverse residual stress with relatively lower magnitude forms at middle part of the weld length and in order to meet static equilibrium, compressive residual stresses are produced at the ends of the weld. Moreover, the effect of stress relieving treatment seems to minimise tensile residual stress and to a certain extent, it can reverse the tensile stress to become compressive as shown in Fig. 5c and d. It is worth noting that the direction and magnitude of residual stresses are important for analysing the crack propagation direction as the weld joints are subjected to external applied stress.

3.3. Corrosion characteristics

Results of potentiodynamic polarisation measurements including corrosion current density (i_o), corrosion rate (CR) and corrosion potential (E_{corr}) for the MIG 5083 aluminium alloy welds in 3.5% NaCl solutions containing various percentages of sodium chromate inhibitor (Na_2CrO_4), namely 0.1, 0.3 and 0.5% are given in Table 4. Based on data in Table 4, the inhibitor efficiency (η) curves for as welded and stress relieved conditions can be calculated using Eq. (3) and the results are shown in Fig. 6. In as welded weld metal, the inhibition efficiency increases steadily as the chromate content increases. In contrast, a small amount of sodium chromate, typically 0.1% is sufficient to dramatically increase the inhibition efficiency up to 50% in stress relieved condition. Subsequently, as the percentage of the chromate is around 0.5%, both the weld metals have the same inhibition efficiency values.

In the present study, the percentage of sodium chromate inhibitor in 3.5% NaCl solutions used for corrosion fatigue tests is determined as 0.3%. The potentiodynamic polarisation curves for as welded and stress relieved weld metals in 3.5% NaCl solutions with and without 0.3% chromate are shown in Fig. 7. Referring to Fig. 7a and Table 4, it can be seen that as welded weld metal does not show active-passive metal since only anodic dissolution occurs with corrosion current density (i_o) is relatively high, typically of 3.78 $\mu A/cm^2$ equivalent to corrosion rate (CR) of 1.6813 mpy. A significant change in the polarisation curves is observed when the weld metal is stress relieved marked by the presence of anodic passivation region and lower corrosion current density, typically of

Table 4
Potentiodynamic polarisation parameters.

Na_2CrO_4 content (%)	As welded weld metal				Stress relieved weld metal			
	E_{corr} (mV)	i_o (μA/cm^2)	*CR* (mpy)	η (%)	E_{corr} (mV)	i_o (μA/cm^2)	*CR* (mpy)	η (%)
0.0	−721.0	3.78	1.6813	0	−863.4	3.48	1.5457	0.0
0.1	−713.1	3.44	1.5269	9.0	−689.7	1.78	0.7984	48.9
0.3	−733.4	2.38	1.0577	37.0	−726.2	1.71	0.7588	50.9
0.5	−713.1	1.78	0.7897	52.9	−746.7	1.59	0.7065	54.3

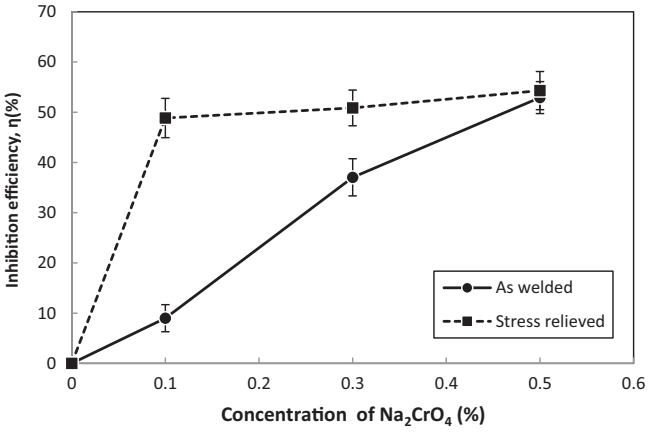

Fig. 6. Inhibition efficiency of chromate for the weld metals with and without stress relieving treatment.

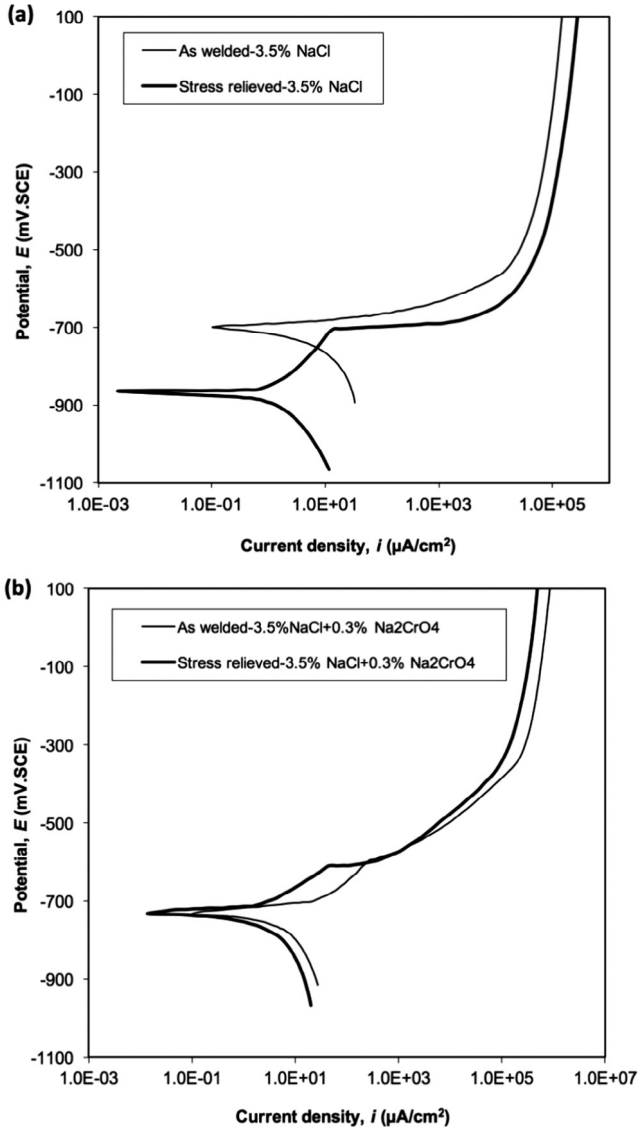

Fig. 7. Polarisation curves for both as welded and stress relieved welds in: (a) Na_2CrO_4-free 3.5%NaCl solutions and (b) 3.5% NaCl solutions with 0.3% Na_2CrO_4.

3.48 μA/cm^2 (1.5457 mpy). The additions of 0.3% Na_2CrO_4 into 3.5% NaCl solutions enhance passivity and further decrease in corrosion current density and corrosion rate for both as welded and stress relieved weld metals as shown in Fig. 7b.

The present investigation has confirmed that stress relieving treatment improved corrosion resistance of the aluminium weld metals, presumably due to the formation of passive film. Two possible factors which are responsible for improving passivity after stress relieving treatment, i.e. first, microstructural change and secondly, compressive residual stress. Since metallurgical factor such as precipitation of β phase (Al_3Mg_2) in AA5083 tends to degrade corrosion performance [3] then compressive residual stress is the most probable factor promoting passivity consistent with previous works [17,18].

3.4. Environmentally assisted fatigue crack propagation behaviour

In the present paper, environmentally assisted fatigue crack propagation behaviours of stress relieved MIG weldedAA5083 joints in 3.5% NaCl solutions have been systematically studied and the results are given in Figs. 8–12. Effect of residual stress on fatigue crack propagation in air can be seen by comparing stress relieved weld metal with as welded condition as shown in Fig. 8. It can be seen that at lower Δ*K*, typically below 7 MPa$\sqrt{m}$, the fatigue crack propagation rate of stress relieved weld metal is lower than that of as welded weld metal then retardation of fatigue crack propagation in stress relieved weld metal occurs at Δ*K* between 9 and 11 MPa$\sqrt{m}$ which is associated with compressive residual stress. Based on superposition approach, the interaction between applied dynamic stress and residual stress determines the total stress. Accordingly, the presence of compressive residual stress reduces the total stress due to subtraction by compressive residual stress. As a result, fatigue crack propagation rate is retarded especially at the early stage of crack propagation. Subsequently, as the crack propagates, the effect of residual stress is diminished.

Fig. 9 shows fatigue crack propagation rates of as welded weld metals under various environments, namely dry air and 3.5% NaCl solutions with and without 0.3% chromate addition. In dry air, as welded weld metal shows relatively low fatigue crack propagation rate. A sharp increase in fatigue crack propagation rate is observed, especially at the early stage of fatigue crack propagation as the weld metal is immersed in 3.5% NaCl solution. Moreover, the addition of 0.3% chromate inhibitor reduces the fatigue crack propagation rate. According to some reports [3,42], chromate can passivate the exposed crack surface and seal off the surface from aggressive environment hence improving resistance to fatigue crack propaga-

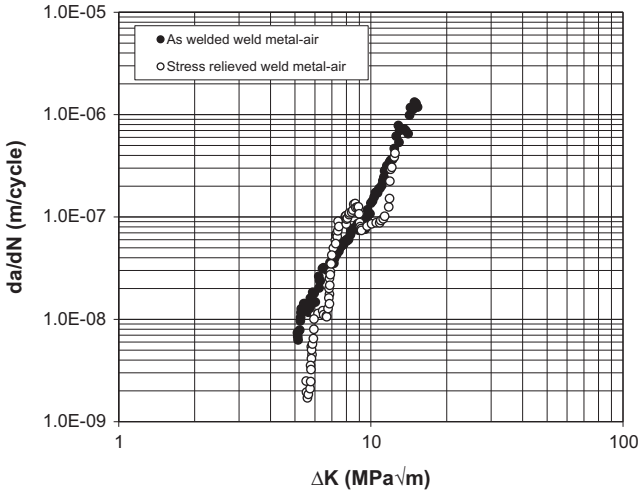

Fig. 8. Effect of residual stress on fatigue crack propagation rates of AA5083 weld metals in air.

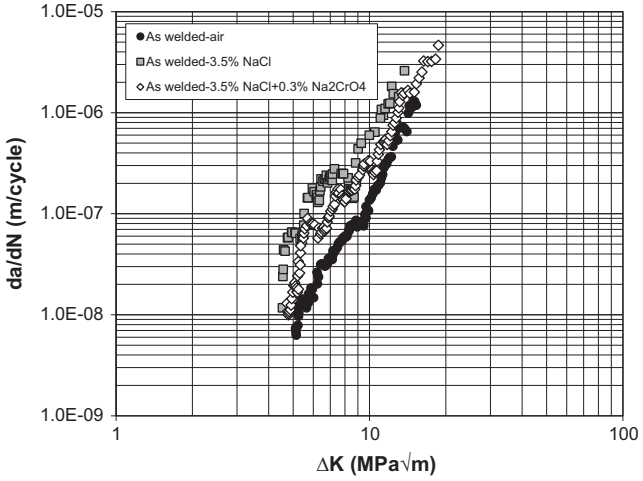

Fig. 9. Fatigue crack propagation rates of as welded AA5083 weld metals in various environments.

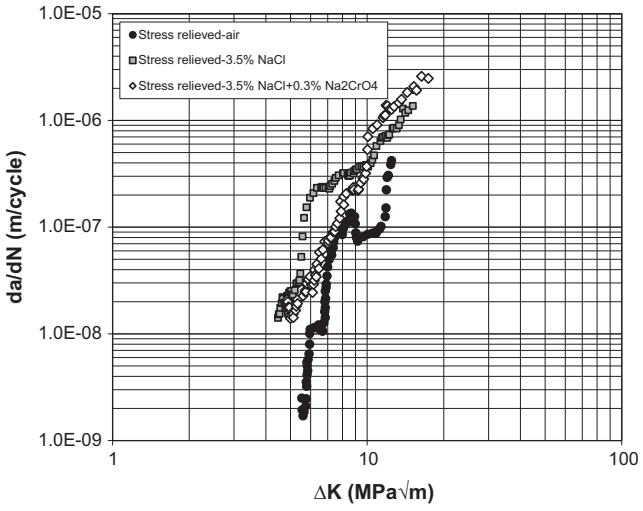

Fig. 10. Fatigue crack propagation rates of stress relieved AA5083 weld metals in various environments.

tion. Similar behaviours are also observed in stress relieved weld metals as shown in Fig. 10. It can be seen that the crack propagation rate of stress relieved weld metal increases with increasing ΔK until a plateau level of approximately 3.10^{-7} m/cycle is achieved at ΔK in the range of 6–10 MPa$\sqrt{m}$. Again, the addition of chromate inhibitor makes the stable crack propagation curve (region II) near stress intensity factor threshold to become linear with no a sharp increase in the crack propagation rate. In comparison with as welded weld metal, the stress relieved weld metal shows better fatigue crack propagation resistance suggesting that the effect of residual stress still exists in corrosive environment.

Results of SEM fractography for both as welded and stress relieved weld metals which are fatigue tested in dry air and a 3.5% NaCl solution are shown in Fig. 11. It can be seen that fractured surface of as welded weld metal reveals poorly defined striations mixed with transgranular cleavage-like fracture as shown in Fig. 11a. This type of fracture is often known as quasi cleavage fracture. Such poorly defined striations in aluminium weld metals are likely associated with the limited possibilities for slips at the crack tip. Again, striation-like fracture is also observed in stress relieved weld metal with finer striation spacings as shown Fig. 11b. Significant changes are observed when as welded and stress relieved weld metals are fatigue tested in a 3.5% NaCl solution marked by the disappearance of striations in both weld metals due to striation dissolution as shown in Fig. 11c and d. In addition, the fractured surfaces of both weld metals reveal corrosion products (light etched) and secondary cracks. There are evidences to suggest that corrosion attacks preferentially on interdendritic spacings resulting in interdendritic debonding, especially in stress relieved weld metal. Results of EDX-microanalysis (Fig. 11e and Fig. 11f) show that chemical compositions of corrosion products for both weld metals are mainly Al, Mg, Si, O, Na and Cl whereas other elements could be considered as contaminants. These elements could be in the forms of Al_2O_3 mixed with Al_3Mg_2 and/or Mg_2Si whilst Na and Cl may come from a NaCl solution.

Fig. 12 shows fatigue fracture surface of stress relieved weld metal in 3.5% NaCl solution containing 0.3%Na_2CrO_4. The fractured surface appears to be cleavage fracture and some regions are suffered from preferential corrosion attacks on interdendritic spacings. Another feature seen in Fig. 12 is the presence of fine particles (appears bright) which are uniformly dispersed throughout the fractured surface. These fine particles are composed of mainly Al and O which may be in the form of Al_2O_3. Unfortunately, the present investigation fails to identify chromium (Cr) but it does not mean that there is not any chromium present at the fractured surface. It can be argued that due to the low percentage of Na_2CrO_4 typically of 0.3%, it is not possible to conduct microanalysis using EDX-ray spectroscopy. Another technique such as Auger electron spectroscopy (AES) as reported by Grilli et al. [43] or electron energy loss spectroscopy (EELS) could solve this problem.

Interactions between residual stress and environment at the crack tip are illustrated in Fig. 13. The effect of residual stress on fatigue crack propagation using superposition approaches has been reported in several works [44–47] and these are summarised as follows. The stress intensity factor range (ΔK) and stress ratio (R) due to the presence of residual stress are calculated as follows:

$$\Delta K_{eff} = (K_{\max} + K_{res}) - (K_{\min} + K_{res}) \quad (4)$$

$$R_{eff} = \frac{K_{\min} + K_{res}}{K_{\max} + K_{res}} \quad (5)$$

According to Eqs. (4) and (5), residual stress does not influence stress intensity factor range (ΔK) and only stress ratio R is affected. However, due to crack closure phenomenon resulted from plastically deformed material at the crack tip, the effect of residual stress is better represented by ΔK_{eff}. According to Elber [48], crack propa-

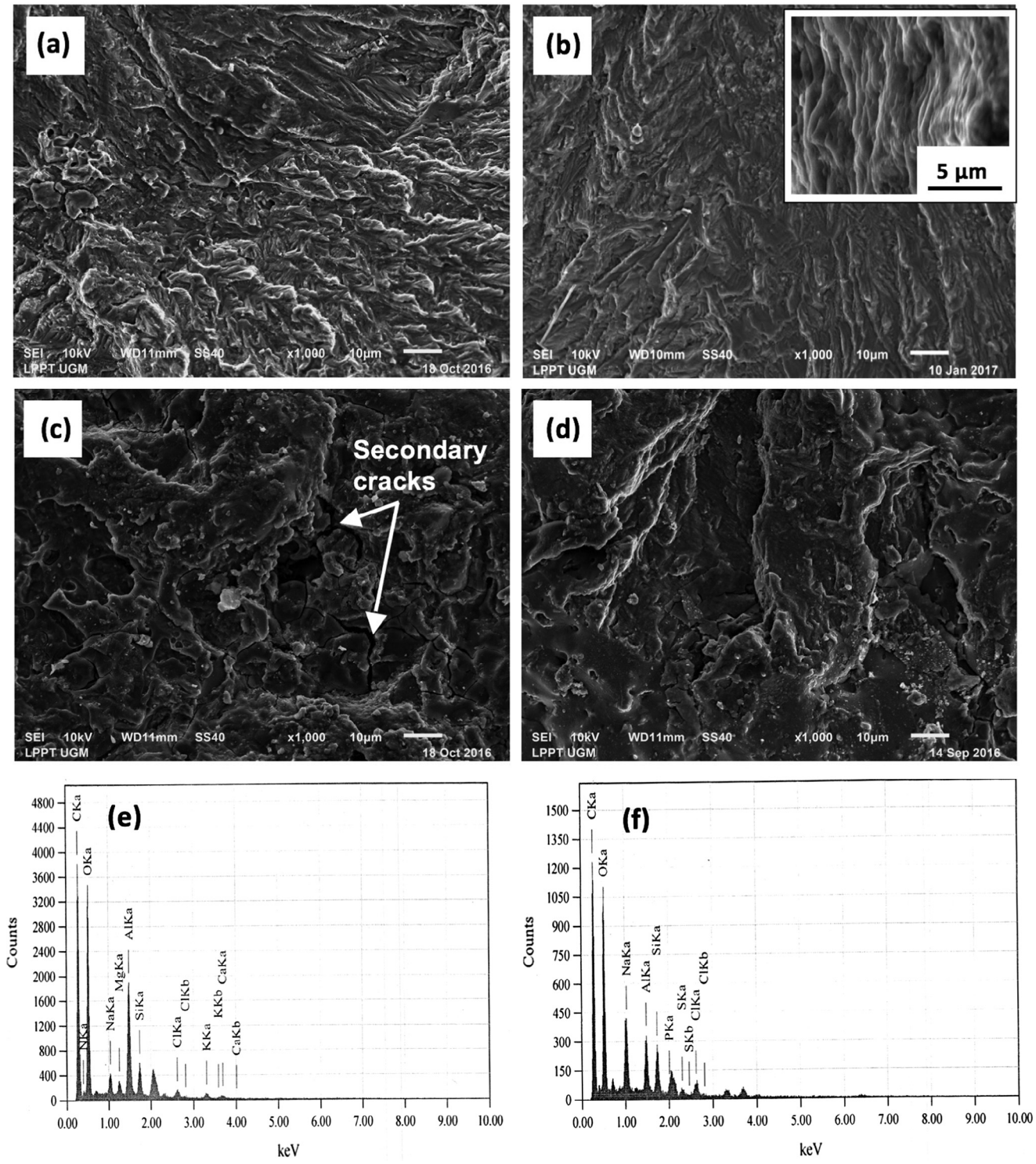

Fig. 11. SEM fractrograpy of MIG weld metals with various conditions: (a) as welded in dry air, (b) stress relieved in dry air with striation-like fracture (inset), (c) as welded in a 3.5% NaCl solution, (d) stress relieved in a 3.5% NaCl solution, and (e), (f) EDX-spectra obtained from (c) and (d) respectively.

gation occurs when the crack tip is fully open at stress intensity factor above K_o where K_o is stress intensity to close the crack. Compressive residual stress results in negative K_{res} and if $|K_{res}| \geqslant K_{\min}$ then the value of $(K_{min} + K_{res})$ is below K_o so that the term $(K_{min} + K_{res})$ is equal to zero. As a result, the reduced stress intensity factor due to crack closure in Eq. (4) can be written as:

$$\Delta K_{eff} = K_{\max} + K_{res} \tag{6}$$

Due to residual stress, the fatigue crack propagation rate (da/dN) is modified as:

$$da/dN = C(\Delta K_{eff})^n \tag{7}$$

where C and n are Paris constants. This equation suggests that the presence of compressive residual stress lowers ΔK_{eff} in favour of fatigue crack propagation inhibition.

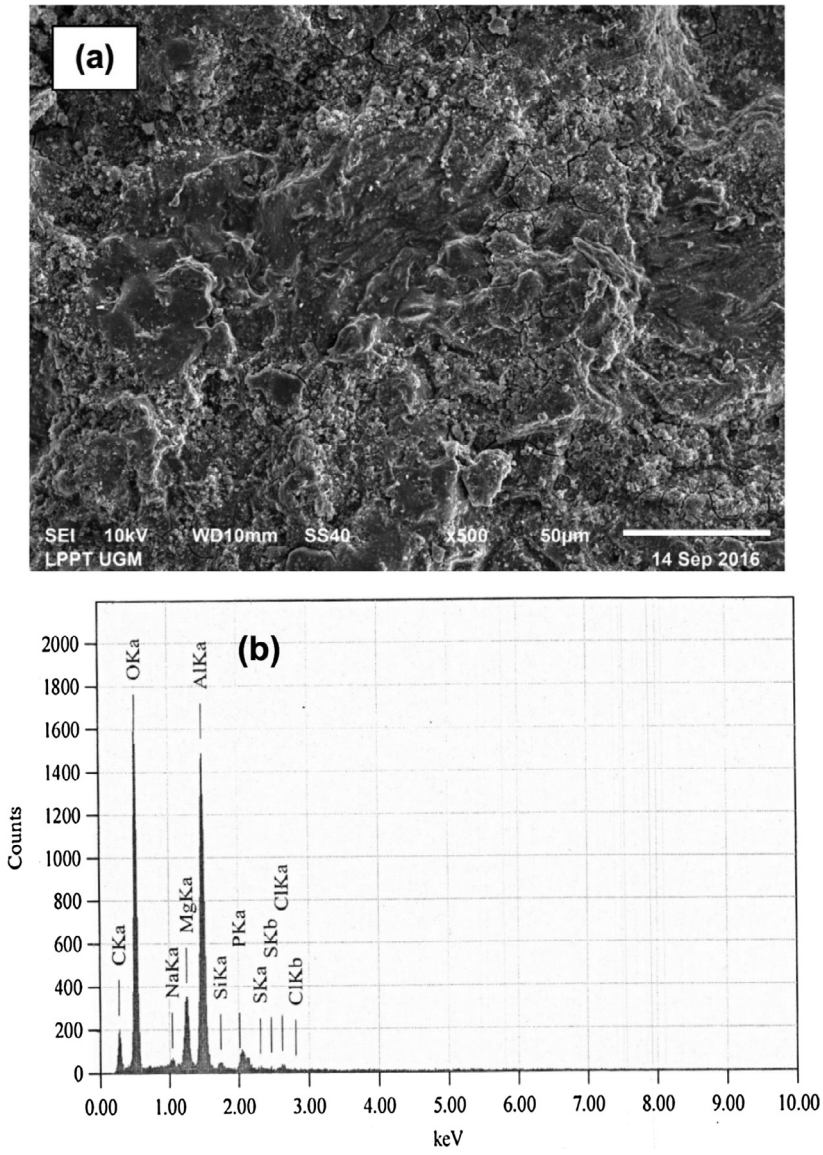

Fig. 12. SEM fractrograpy of stress relieved MIG weld metal in 3.5%NaCl containing 0.3% Na_2CrO_4 showing intergranular fatigue crack surface with EDX-spectra taken from the fractured surface.

As mentioned previously, compressive residual stress could be linked to stability of passive film, probably in the form of Al_2O_3 which contributed to lower corrosion rate. However, this passive film can be destroyed by aggressive ions such as chloride in 3.5% NaCl solution. The deleterious effect of aqueous environment on fatigue crack propagation has been reported by a number of some researchers [15,42,49] and their findings may apply to AA5083 welds. As the passive film of AA5083 welds at the crack tip is destroyed by slips and chloride ions, then dissolution of the aluminium weld metal takes place as follows:

$$Al \rightarrow Al^{3+} + 3e^{-} \quad (8)$$

The hydrolisis of metal cations may occur resulting in low pH, i.e.:

$$Al^{3+} + H_2O = Al(OH)^{2+} + H^{+} \quad (9)$$

Hydrogen ions are then diffused into the weld metal ahead of the crack tip and cause hydrogen embrittlement. As a result, fatigue crack propagation rate increases especially at the beginning of crack propagation.

Results of the present investigation have confirmed that the presence of chromate inhibits corrosion attacks. This inhibition effect of chromate can be accounted for based on its capability of oxidising aluminium (Al) due to reduction of Cr (VI) to form Cr (III) at pH neutral according to the following reactions [27]:

$$2Al + Cr_2O_7^{2-} + 8H^{+} \rightarrow 2Cr(OH)_3 + H_2O + 2Al^{3+} \quad (10)$$

$$2Al + 2HCrO_4^{-} + 8H^{+} \rightarrow Cr_2O_3 \cdot 3H_2O + 2H2O + 2Al^{3+} \quad (11)$$

Reactions above are expected to form a thin layer of chromium oxide (Cr_2O_3) which provides a barrier to further dissolution. At pH of 5 or above, this chromium oxide is thermodynamically stable. This passive film at the crack tip may be broken as the crack is open but it can reform at sufficiently low frequency. In such a condition, the fatigue crack propagation rate is dependent on competition between kinetics of depassivation by slip and repassivation resulted from the formation of thin layer of oxide.

The fractographic results have shown that fatigue crack propagates transgranularly in 3.5% NaCl solution. The use of stress relieving treatment and inhibitor addition seems to promote, at a lesser

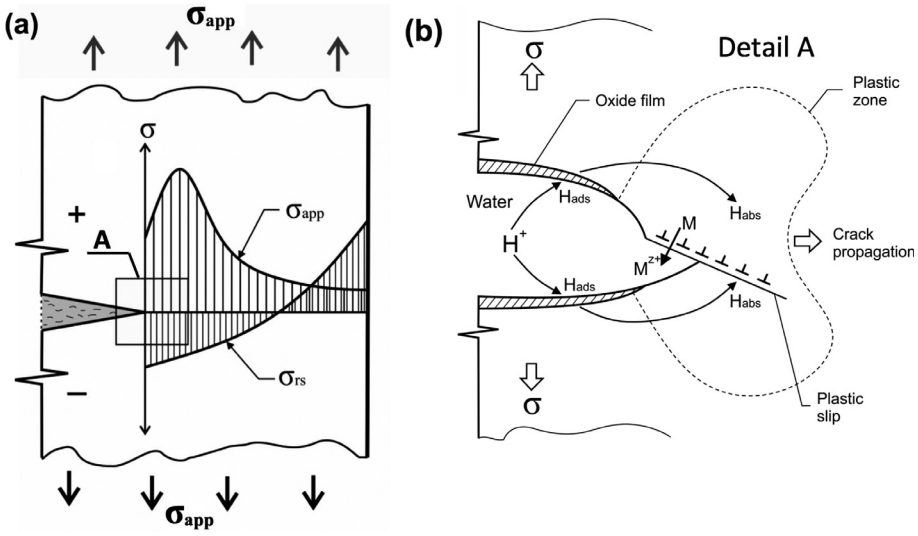

Fig. 13. Proposed mechanism of environmentally assisted fatigue crack propagation: (a) distribution of applied (σ_{app}) and residual (σ_{res}) stresses at a crack tip and (b) magnified picture of a crack tip outlined by square A in (a) showing interactions between anodic dissolution, hydrogen effects and formation of protective films at the crack tip.

extent, intergranular paths in which the crack propagates along interdendritic spacings as shown in Figs. 11d and 12. It seems that due to the lack of protective oxide film at the crack tip as shown in as welded weld metal, fatigue fracture mechanism takes place through hydrogen embrittlement mechanism resulting in transgranular fatigue fracture as previously discussed. However, as the crack tip is isolated by thin oxide film then the hydrogen diffusion into the weld metal in front of the crack tip is inhibited and a result, another lower energy path for crack propagation is probably operative. It may be argued that interdendritic spacings are preferred sites for segregation and they are anodic to the surrounding dendritic grains (α-phase). Such a condition can create localised galvanic cells and anodic corrosion occurs preferentially on the interdendritic spacings leading to anodic dissolution of β-phase. This may provide low fatigue crack propagation resistance and a result, intergranular fatigue crack propagation occurs in competition with the transgranular crack.

It can be summarised that the effects of residual stress when the stress is compressive, observed in the present investigation are two-fold. First, compressive residual stress changes electrochemical corrosion properties in favour of passive film formation and secondly, compressive residual stress reduces stress intensity factor range (ΔK_{eff}) hence lowering the fatigue crack propagation.

According to Eq. (5), the presence of residual stress changes stress ratio (R) resulting in R_{eff} whereas corrosive environment seems to reduce intensity factor threshold (ΔK_{th}). By considering these two factors, Wang et al. [50] have proposed a model which combines Walker model and Trantina-Johnson equation for environmentally assisted fatigue crack propagation rate near threshold region and stable crack propagation rate region as:

$$da/dN = C(\Delta K_{eff} - \Delta K_{th})^{n_1}(1 - R_{eff})^{n_2} \quad (12)$$

where n_1 and n_2 are the material constant.

Another important factor which influences environment fatigue is loading frequency. It has been reported that environment fatigue crack propagation rates increase as the frequency decreases since lower frequency gives more time per loading cycle which enables electrochemical reactions to occur [51]. In the case of active-passive metals such as aluminium alloys or in inhibitor-containing environment, lower frequency provides sufficient time for metals to repassivate due to oxide passive film formation [20,52]. This oxide film isolates the metal surface from corrosive environment hence resulting in environment crack inhibition. It seems that this factor should be taken into account as suggested by Kitsunai et al. [53] and a modified model which incorporates the loading frequency is proposed as:

$$da/dN = FC(\Delta K_{eff} - \Delta K_{th})^{n_1}(1 - R_{eff})^{n_2} \quad (13)$$

where F is the loading frequency dependency factor and its value is dependent on combined effect of frequency and environment. The modified model is expected to provide reasonable prediction for remaining life of structural metals subjected to environmentally assisted fatigue crack propagation.

4. Conclusions

Environmentally assisted fatigue crack propagation behaviours of MIG A5083 welds in 3.5% NaCl solution under stress relieving treatment, namely static thermal tensioning were studied and the conclusions that can be drawn from this investigation are as follows:

- Stress relieving treatment using static thermal tensioning can produce compressive residual stress which enhances the formation of passive film as indicated by the presence of passive regions in potentiodynamic polarisation curves accompanied by lower current densities.
- Apart from compressive residual stress, the ability of repassivation increases with the addition of inhibitor such as chromate.
- Inhibition of environmentally assisted fatigue crack propagation in the weld metals under stress relieving treatment is associated with synergistic effect of compressive residual stress which lowers ΔK and ability of the weld metals to repassivate.

Acknowledgements

The authors are grateful to Kemenristek-DIKTI and UGM for providing research grant, named STRANAS under contract number: 960/UN1-P.III/LT/DIT-LIT/2016.

References

[1] Perel VY, Misak HE, Mall S, Jain VK. Biaxial fatigue crack growth behavior in aluminium alloy 5083-H116 under ambient laboratory and saltwater environments. J Mater Eng Perform 2015;24(4):1565–72.
[2] Abkenar MR, Kihl DP, Manzari MT. Fatigue tests on aluminium specimens subjected to constant and random amplitude loadings. ASME J Mater Technol 2016;138:1–7.
[3] Holtz RL, Pao PS, Bayles RA, Longazel TM, Goswami R. Corrosion fatigue of aluminium alloy 5083-H131 sensitizes at 448 K (175 °C). Metal Mater Trans A 2012;43A:2839–49.
[4] Costa JDM, Jesus JS, Loureiro A, Ferreira JAM, Borrego LP. Fatigue life improvement of mig welded aluminum T-joints by friction stir processing. Int J Fatigue 2014;61:244–54.
[5] Messler Jr RW. Principles of welding: processes, physics, chemistry and metallurgy. 1st ed. New York: John Wiley & Sons; 1999.
[6] Altenkirch J, Steuwer A, Peel MJ, Wither PJ, Williams SW, Poad M. Mechanical tensioning of high strength aluminum alloy friction stir welds. Metal Mater Trans A 2008;39A:3246–59.
[7] Jose MJ, Kumar SS, Sharma A. Vibration assisted welding processes and their influence on quality of welds. Sci Technol Weld Join 2016;21(4):243–58.
[8] Xu D, Liu XS, Wang P, Yang JG, Fang HY. New technique to control welding buckling distortion and residual stress with non-contact electromagnetic impact. Sci Technol Weld Join 2009;14(8):753–9.
[9] Michaleris P, Sun X. Finite element analysis of thermal tensioning techniques mitigating weld buckling distortion. Weld J 1997;76(22):451–7.
[10] Ilman MN, Kusmono, Muslih MR, Subeki N, Wibowo H. Mitigating distortion and residual stress by static thermal tensioning to improve fatigue crack growth performance of MIG AA5083 welds. Mater Des 2016;99:273–83.
[11] Mochizuki M, Toyoda M. Weld distortion control during welding process with reverse-side heating. ASME J Pressure Vessel Technol 2007;129:619–29.
[12] Han WT, Wan FR, Li G, Dong CL, Tong JH. Effect of trailing heat sink on residual stresses and welding distortion in friction stir welding Al sheets. Sci Technol Weld Join 2011;16(5):453–8.
[13] Cheng X, Fisher JW, Prask HJ, Gnaupel-Herold T, Yen BT, Roy S. Residual stress modification by post-weld treatment and its beneficial effect on fatigue strength of welded structures. Int J Fatigue 2003;25:1259–69.
[14] Ipekoglu G, Cam G. Effects of initial temper condition and post weld heat treatment on the properties of dissimilar friction-stir-welded joints between AA7075 and AA6061 aluminium alloys. Metal Mater Trans A 2014;45:3074–87.
[15] Proton V, Alexis J, Andrieu E, Delfosse J, Lafont MC, Blanc C. Characterisation and understanding of the corrosion behaviour of the nugget in a 2050 aluminium alloy friction stir welding. Corros Sci 2013;73:130–42.
[16] Wang H, Yu C, Huang S. Effect of heat treatment on mechanical property and electrochemical corrosion behavior of X65 pipeline steel in 3.5 wt.% NaCl. Int J Electrochem Sci 2015;10:5827–41.
[17] Trdan U, Grum J. Evaluation of corrosion resistance of AA6082-T651 aluminium alloy after laser shock peening by means of cyclic polarisation and EIS methods. Corros Sci 2012;59:324–33.
[18] Peyre P, Scherpereel X, Berthe L, Carboni C, Fabbro R, Beranger G, et al. Surface modifications induced in 316L steel by laser peening and shot-peening. Influence on pitting corrosion resistance. Mater Sci Eng, A 2000;280:294–302.
[19] Dhinakaran S, Prakash RV. Effect of low cyclic frequency on fatigue crack growth behavior of a Mn-Ni-Cr steel in air and 3.5% NaCl solution. Mater Sci Eng, A 2014;609:204–8.
[20] Rozali S, Mutoh Y, Nagata K. Effect of frequency on fatigue crack growth behavior of magnesium alloy AZ61 under immersed 3.5 mass% NaCl environment. Mater Sci Eng, A 2011;528:2509–16.
[21] Tada E, Noda K, Kumai S, Tsuru T. The effect of straining frequency and stress ratio on polarization current responded to cyclic strain in a commercial iron. ISIJ Int 1997;37(12):1189–96.
[22] Duff JA, Marrow TJ. In situ observation of short fatigue crack propagation in oxygenated water at elevated temperature and pressure. Corros Sci 2013;68:34–43.
[23] Burns JT, Gangloff RP. Effect of low temperature on fatigue crack formation and microstructure-scale growth from corrosion damage in Al-Zn-Mg-Cu. Metal Mater Trans A 2013;44A:2083–105.
[24] Thomas JP, Wei RP. Corrosion fatigue crack growth of steels in aqueous solutions I: experimental results and modeling the effects of frequency and temperature. Mater Sci Eng, A 1992;159:205–21.
[25] Ryl J, Wysocka J, Jarzynka M, Zielinski A, Orlikowski J, Darowicki K. Effect of native air-formed oxidation on the corrosion behavior of AA 7075 aluminium alloys. Corros Sci 2014;87:150–5.
[26] Marlaud T, Malki B, Henon C, Deschamps A, Baroux B. Relationship between alloy composition, microstructure and exfoliation corrosion in Al-Zn-Mg-Cu alloys. Corros Sci 2011;53:3139–49.
[27] Palcut M, Priputen P, Kusy M, Janovec J. Corrosion behaviour of Al-29at% Co alloy in aqueous NaCl. Corros Sci 2013;75:461–6.
[28] Pao PS, Holtz RL, Jones HN, Feng CR. Effect of environment on fatigue crack growth in ultrafine grain Al-Mg. Int J Fatigue 2009;31:1678–83.
[29] Bonakdar A, Wang F, Williams JJ, Chawla N. Environmental effects on fatigue crack growth in 7075 aluminium alloy. Metal Mater Trans A 2012;43A:2799–809.
[30] Mikheevskiy S, Glinka G, Lee E. Fatigue crack growth analysis under spectrum loading in various environmental conditions. Metal Mater Trans A 2013;44A:1301–10.
[31] Sarrazin-Baudox C, Loubat F, Potiron S. On the role of water vapor and oxygen on the fatigue crack propagation behavior at 550 °C of a Ti 6242 alloy. Metal Mater Trans A 2006;37A:1201–9.
[32] Huneau B, Mendez J. Fatigue behavior of a high strength steel in vacuum, in air and in 3.5% NaCl solution under cathodic protection. Mater Sci Eng, A 2003;345:14–22.
[33] deVries SB, Baker A, Janssen GCAM, deWit H. Fatigue crack initiation behavior of welded AA5083 in seawater environment. ASME J Eng Mater Technol 2004;126:199–203.
[34] Mutombo K, du Toit M. Corrosion fatigue behaviour of aluminium alloy 6061-T651 welded using fully automatic gas metal arc welding and ER5183 filler alloy. Int J Fatigue 2011;33:1539–47.
[35] Sharma MM, Tomedi JD, Parks JM. A microscopic study on the corrosion fatigue of ultra-fine grained and conventional Al-Mg alloy. Corros Sci 2015;93:180–90.
[36] Pratihar S, Turski M, Edwards L, Bouchard PJ. Neutron diffraction residual stress measurements in a 316L stainless steel bead-on-plate weld specimen. Int J Press Vessels Pip 2009;86:13–9.
[37] Scendo M. Inhibition of copper corrosion in sodium nitrate solutions with nontoxic inhibitors. Corros Sci 2008;50:1584–92.
[38] Li X, Deng S, Fu H. Sodium molybdate as a corrosion inhibitor for aluminium in H_3PO_4 solution. Corros Sci 2011;53:2748–53.
[39] Thretewey KR, Chamberlain J. Corrosion for science and engineering. 2nd ed. Essex: Longman; 1995.
[40] Guan Q. Control of buckling distortion in plates and shells, In: Feng Z editor. Processes and mechanisms of welding residual stress and distortion. 1st ed. Cambridge: Woodhead Publishing Limited; 2005. p.295–343.
[41] Michaleris P. Introduction to welding residual stress and distortion, In: Michaleris P editor. Minimization of welding distortion and buckling: Modelling and implementation. 1st ed. Cambridge: Woodhead Publishing Limited; 2011. p. 1–21.
[42] Ilman MN. Chromate inhibition of environmentally assisted fatigue crack propagation of aluminium alloy AA 2024-T3 in 3.5% NaCl. Int J Fatigue 2014;62:228–35.
[43] Grilli R, Baker MA, Castle JE, Dunn B, Watts JF. Corrosion behaviour of a 2219 aluminium alloy treated with a chromate conversion coating exposed to a 3.5% NaCl solution. Corros Sci 2011;53:1214–23.
[44] La Rue JE, Daniewicz SR. Predicting the effect of residual stress on fatigue crack growth. Int J Fatigue 2007;29:508–15.
[45] Lammi CJ, Lados DA. Effects of processing residual stresses on fatigue crack growth behavior of structural materials: experimental approaches and microstructural mechanisms. Metall Mater Trans A 2012;43A:87–107.
[46] Ritchie RO. Mechanisms of fatigue-crack propagation in ductile and brittle solids. Int J Fract 1999;100:55–83.
[47] Ma YE, Staron P, Fischer T, Irving PE. Size effects on residual stress and fatigue crack growth in friction stir welded 2195-T8 aluminium-Part II: modelling. Int J Fatigue 2011;33:1426–34.
[48] Elber W. Fatigue crack closure under cyclic tension. Eng Fract Mech 1970;2:37–45.
[49] Magnin T. Fatigue crack initiation: effect of environment. encyclopedia of materials: science and technology. NY: Springer; 2001. p. 2877–82.
[50] Wang CQ, Xiong JJ, Shenoi RA, Liu MD, Liu JZ. A modified model to depict corrosion fatigue crack growth behavior for evaluating residual lives of aluminium alloys. Int J Fatigue 2016;83:280–7.
[51] Gangloff RP. Fatigue crack propagation in aerospace aluminium alloys. J Aircraft 1994;31(3):720–9.
[52] Warner JS, Gangloff RP. Molybdate inhibition of corrosion fatigue crack propagation in precipitation hardened Al–Cu–Li. Corros Sci 2012;62:11–21.
[53] Kitsunai Y, Tanaka M, Yoshihisa E. Influence of residual stresses and loading frequencies on corrosion fatigue crack growth behavior of weldments. Metall Mater Trans A 1998;29A:1289–98.